infrastructures

MDPI

Article

Collision Milling of Oil Shale Ash as Constituent Pretreatment in Concrete 3D Printing

Lucija Hanžič [1,*], Mateja Štefančič [1], Katarina Šter [1], Vesna Zalar Serjun [1], Māris Šinka [2], Alise Sapata [2], Genādijs Šahmenko [2], Evaldas Šerelis [3], Baiba Migliniece [4] and Lidija Korat Bensa [1]

1 Slovenian National Building and Civil Engineering Institute (ZAG), SI-1000 Ljubljana, Slovenia; mateja.stefancic@zag.si (M.Š.); katarina.ster@zag.si (K.Š.); vesna.zalar@zag.si (V.Z.S.); lidija.korat@zag.si (L.K.B.)
2 Institute of Sustainable Building Materials and Engineering Systems, Riga Technical University (RTU), LV-1048 Riga, Latvia; maris.sinka@rtu.lv (M.Š.); alise.sapata@rtu.lv (A.S.); genadijs.sahmenko@rtu.lv (G.Š.)
3 Faculty of Civil Engineering and Architecture, Kaunas University of Technology (KTU), 51367 Kaunas, Lithuania; evaldas.serelis@ktu.lt
4 Sakret, LV-2121 Rumbula, Latvia; baiba.migliniece@sakret.lv
* Correspondence: lucija.hanzic@zag.si; Tel.: +386-2-330-2422

Abstract: Concrete is an essential construction material, and infrastructures, such as bridges, tunnels, and power plants, consume large quantities of it. Future infrastructure demands and sustainability issues necessitate the adoption of non-conventional supplementary cementitious materials (SCMs). At the same time, global labor shortages are compelling the conservative construction sector to implement autonomous and digital fabrication methods, such as 3D printing. This paper thus investigates the feasibility of using oil shale ash (OSA) as an SCM in concrete suitable for 3D printing, and collision milling is examined as a possible ash pretreatment. OSA from four different sources was collected and analyzed for its physical, chemical, and mineralogical composition. Concrete formulations containing ash were tested for mechanical performance, and the two best-performing formulations were assessed for printability. It was found that ash extracted from flue gases by the novel integrated desulfurizer has the greatest potential as an SCM due to globular particles that contain β-calcium silicate. The 56-day compression strength of concrete containing this type of ash is ~60 MPa, the same as in the reference composition. Overall, collision milling is effective in reducing the size of particles larger than 10 µm but does not seem beneficial for ash extracted from flue gasses. However, milling bottom ash may unlock its potential as an SCM, with the optimal milling frequency being ~100 Hz.

Keywords: digital concrete; 3D printing; oil shale ash; supplementary cementitious material; collision milling

Academic Editor: Patricia Kara De Maeijer

Received: 15 November 2024
Revised: 24 December 2024
Accepted: 30 December 2024
Published: 13 January 2025

Citation: Hanžič, L.; Štefančič, M.; Šter, K.; Zalar Serjun, V.; Šinka, M.; Sapata, A.; Šahmenko, G.; Šerelis, E.; Migliniece, B.; Korat Bensa, L. Collision Milling of Oil Shale Ash as Constituent Pretreatment in Concrete 3D Printing. *Infrastructures* **2025**, *10*, 18. https://doi.org/10.3390/infrastructures10010018

1. Introduction

The construction sector is notorious for a conservative approach to change and, consequently, a low level of innovation compared to other industry sectors. On one hand, its inherent attributes, such as site-based operations, project-based business models, and complex value chains, make it difficult to measure innovation returns using criteria from other industries [1]. On the other hand, it has been asserted that construction firms do not need to innovate to remain successful or viable [2] and that historically, the construction sector has ignored investments in research and development [3]. As a consequence, the level of automation in construction is low. However, workforce issues, such as aging [4], a shortage of young talent due to poor industry image [3], and poor representation of women [5,6],

are pressing the industry into adopting less labor-intensive and more attractive fabrication methods. These challenges call for a paradigm shift presented in *Construction 4.0* formwork [3] with digitalization as its core component.

Digitalization in construction became a hot topic in the 1990s due to a pressing need to digitally exchange data already created by digital means. As a result, Building Information Models and Digital Twins emerged [7,8]. However, it took the construction industry almost another 20 years to start considering digital means for translating digital objects into physical ones. One of the most promising technologies for large-scale digital construction is the additive manufacturing of concrete structures, colloquially referred to as 3D concrete printing. Its exponential growth has resulted in a rather unprecedented leapfrog in the Technology Readiness Level (TRL), which is currently estimated to be between 6 and 7 [9]. To achieve full market implementation of TRL9, a number of challenges still need to be addressed [10–14]. In this respect, three areas of expertise have been recognized as crucial [13], namely, (i) digital modeling and printer operation, (ii) engineering of mechanical components, and (iii) material functionalities.

One of the central issues related to the material functionalities is that in terms of the material per-unit consumption, printed structures have a considerably worse carbon footprint than the structures they are replacing [12]. One of the reasons is the high paste content, of which cement is the major component [12]. Therefore, replacing clinker, which is the primary constituent of cement, with supplementary cementitious materials (SCMs) is considered to have huge potential [15,16]. The problem is a limited supply of conventional SCMs, in particular, fly ash (FA) and ground granulated blast furnace slag (GGBS) [16]. Thus, alternative sources of SCMs need to be investigated. One such source is oil shale ash (OSA), a residue of power plants using oil shale as an energy source.

The use of oil shale in power plants is not as widespread as the use of coal; however, in a few countries, such as Estonia, it is an important natural resource primarily consumed by power plants [17]. The annual amount of OSA formed in the combustion process in Estonia alone is estimated to be about 5–7 Mt, and the majority of it is deposited in stockpiles in the vicinity of power plants [18]. While OSA is a considerably different material than FA, its potential for use in construction materials [19] and, in particular, in concrete [20–22] has already been demonstrated, and Estonian standard EVS 927 [23] for specification, performance, and conformity of OSA for building materials was published in 2018.

The characterization of six OSA streams established [19] that the principal constituents of OSA are SiO_2, CaO, and Al_2O_3, forming the following major minerals: calcite, K-feldspar, quartz, and lime. Also present are two cementitious minerals, namely, dicalcium silicate (C_2S) and tetracalcium aluminoferrite (C_4AF). Furthermore, the specific surface area and the mean particle size were found to be ~1–6 $m^2\ g^{-1}$ and ~20–45 μm, respectively.

The fineness of OSA compares favorably to cement whose specific surface area is ~0.01–1 $m^2\ g^{-1}$ and whose particle sizes range between ~5 and 80 μm [24]. In concrete, fine powders together with water and admixtures form the paste and, as mentioned above, high paste content is required for printable concrete. Namely, the paste provides the necessary cohesiveness to the mix, with the size and morphology of the powder particles playing a crucial role [25]. In principle, the smaller the particles, the more pronounced the cohesive forces and, therefore, reducing their size by milling or grinding can prove beneficial.

It has been reported [26] that collision milling is an effective method to reduce the particle size of brittle materials. It has been successfully employed in the pretreatment of quartz and dolomite sand used as aggregate in cement-based mortar. Despite the sand being considered an inert component, the compressive strength of the mortar increased if the milled sand was used immediately after grinding [27]. However, if the sand was exposed to environmental conditions for 28 days before being mixed into mortar, the

strength decreased compared to mortar with untreated sand [27]. This indicates that collision milling might activate the material.

This paper thus aims to assess the performance of OSA in concrete mixtures for extrusion 3D printing and collision milling as a pretreatment for OSA. It is hypothesized that reducing the particles' size can improve the printability of concrete mixtures and possibly activate the ash, thus improving the mechanical characteristics of concrete. The focus of this study is the characterization of different types of OSA, the identification of the most suitable ash for concrete 3D printing applications, and the proof of concept on a laboratory-scale gantry printer. The formulation, optimization, and detailed assessment of printable concrete compositions, as well as their viability, are out of the scope of this work.

Additionally, it should be stressed that this paper showcases how digital fabrication can address the industry challenges related to workforce shortages and attract women and young people to construction jobs. Namely, seven out of the ten authors of this paper are women, and two of them are early-stage researchers, while another five authors were awarded a PhD within the last ten years.

2. Materials and Methods

In pursuance of the aims identified above, the following investigation methodology was implemented:

1. Collection of OSA from three power plants;
2. Pretreatment of OSA with collision milling in a laboratory-scale disintegrator;
3. Physical, chemical, and mineralogical characterization of OSA before and after pretreatment;
4. Design of printable concrete compositions containing OSA;
5. Proof of concept—testing the strength and printability of a small number of concrete compositions.

The ash samples were collected at selected power plants and were bagged, sealed, and brought to *Riga Technical University* (RTU) laboratories for further processing. They were split into two portions—one was retained in its original condition without pretreatment while the other was collision milled. The original and processed ash samples were sent to the *Slovenian National Building and Civil Engineering Institute* (ZAG) laboratories for characterization, which comprises physical, chemical, and mineralogical analysis. Furthermore, the ash samples were used in concrete mixtures at RTU to assess mechanical properties and printability.

2.1. Oil Shale Ash

The OSA was collected at three power plants, namely, *Eesti Elektrijaam*, *Enefit280 Elektrijaam*, and *Auvere Elektrijaam*. The first two use only oil shale as fuel while the latter combines oil shale with wood. At all plants, the fly ash was collected, while at the *Auvere* plant, the bottom ash (ba) was also collected. The fly ash at the *Eesti* plant is extracted by a novel integrated desulfurizer (nid), while at *Enefit280* and *Auvere*, the extraction is carried out by electrostatic filters (ef). The ash samples were collected from the silos located at the power plant sites where the ash is temporarily stored. The information about ash sources and assigned designations are summarized in Table 1. Photographs of unprocessed ash are collated in Figure 1.

Table 1. Oil shale ash collected for this study.

Ash Designation	Power Plant	Fuel	Ash Extraction Point	Ash Type
OSA-Ees(nid)	Eesti	Oil shale	Novel integrated desulfurizer	Fly ash
OSA-Ene(ef)	Enefit280	Oil shale	Electrostatic filter	Fly ash
OSWA-Auv(ef)	Auvere	Oil shale and wood	Electrostatic filter	Fly ash
OSWA-Auv(ba)	Auvere	Oil shale and wood	Grate	Bottom ash

Figure 1. Macrophotographs of collected ash. Notation: Ash: OSA—oil shale ash, OSWA—oil shale + wood ash; power plants: Ees—*Eesti*, Ene—*Enefit280,* and Auv—*Auvere*; ash extraction method: nid—novel integrated desulfurizer, ef—electrostatic filters, ba—bottom ash.

2.2. Collision Milling Pretreatment

The pretreatment of ash by collision milling was executed on a laboratory-scale disintegrator *Desi-11* shown in Figure 2. The central unit of the disintegrator is the milling chamber, which is hermetically sealed during the operation. It houses two vertical rotors driven in opposite directions by asynchronous electric motors, which generate a nominal rotation speed of 3000 rpm. The rotation speed is controlled through the frequency converters and can be adjusted in the range of ±100 % of the nominal speed. The rotors are fitted with grinding discs whose concentrically shaped segments are spaced in such a way that segments of one disk fit between the segments of the other disk.

Before milling, the ash was dried at 80 °C for 24 h and cooled to room temperature. It was fed into the milling chamber via the loading hopper at a flow rate of ~170–200 g min^{-1}. Bottom ash OSWA-Auv(ba), which is the coarsest, as seen in Figure 1, was milled first, and a range of frequencies was tested, namely, 30, 50, 100, or 130 Hz. These frequencies correspond to the tangential speed of ~14, 24, 47, and 61 m s^{-1}, respectively, considering the disk diameter is 150 mm. Based on preliminary research on OSA extracted from the flue gases and the results obtained on OSWA-Auv(ba), the milling frequency of 100 Hz was selected for OSA-Ees(nid), OSA-Ene(ef), and OSWA-Auv(ef). The milled material is discharged into a sealed collection vessel. The time required to mill a batch of ~700 g of ash was 5–10 min. Table 2 summarizes the ash treatment and designations.

Table 2. Summary of ash pretreatment by collision milling and milled sample designations.

Ash Designation	Milling Frequency (Hz)	Milled Ash Designation
OSA-Ees(nid)	100	OSA-Ees(nid)/100
OSA-Ene(ef)	100	OSA-Ene(ef)/100
OSWA-Auv(ef)	100	OSWA-Auv(ef)/100
OSWA-Auv(ba)	30	OSWA-Auv(ba)/30
	50	OSWA-Auv(ba)/50
	100	OSWA-Auv(ba)/100
	130	OSWA-Auv(ba)/130

Figure 2. Laboratory-scale disintegrator *Desi-11* for collision milling. Labeled parts: 1—disintegrator with an open milling chamber showing rotors and grinding disks; 2—vibro feeder with a hopper; 3—air filter; 4—receiving container; and 5—control board.

2.3. Characterization of OSA

2.3.1. Physical Characteristics

The following physical characteristics of the ash specimens were determined:

- Moisture content;
- Particle density;
- Particle size distribution (PSD);
- Particle morphology.

The first two characteristics were measured only on the unprocessed material.

Moisture content was determined on the as-received materials according to standard EN 1097-5 [28]. A test portion of ~20–50 g was scooped from the bag, and its mass was immediately determined. Next, it was dried at 110 °C to a constant mass and cooled in a desiccator to room temperature. Finally, the mass of the dry test portion was determined, and the moisture content (wt%) was calculated against the dry mass.

Particle density was measured by the pycnometer method following standard EN 1097-7 [29]. A test portion of ~20 g was scooped from the bagged material and dried before being loaded into the 1.8 cm^3 cell of the helium pycnometer *Quantachrome Ultrapyc 1200e*. The instrument flow purge was set to 1.0 min, and at least three measurements were automatically performed. If there was a larger discrepancy between the results, the instrument automatically took further measurements until the deviation between the results was sufficiently small. Hence, up to five measurements were recorded on some test portions.

The PSD was determined by laser diffraction in compliance with standard ISO 13320 [30] using the *Microtrac SYNC 5001* instrument. One test portion of ~1 g was scooped

from the bag, loaded into the test cell, and analyzed using a wet configuration in isopropanol. For comparison purposes, the PSD of cement CEM I was also measured.

The morphology of the ash particles was analyzed by scanning electron microscopy (SEM). Specimens were prepared by scooping material from the bag and tapping it onto ~1 cm^2 of the double-sided conductive carbon tape attached to the standard SEM stand. The specimens were examined with the *JEOL IT500 LV* microscope equipped with a Wolfram filament. The microscope was operated at an accelerating voltage of 15 kV in a low vacuum mode at a working distance of ~10 mm.

2.3.2. Chemical Characteristics

In terms of chemical characteristics of OSA, the following were analyzed:

- Elemental composition;
- Free calcium oxide (CaO);
- Soundness;
- Chemical reactivity.

The first three characteristics were determined only on unprocessed ash.

In the scope of elemental composition, the loss on ignition (LOI) was performed first, according to the method specified by standard EN 196-2 [31]. A change in mass of ~1 g test portion was determined after successive 15 min ignitions at 950 °C. Afterwards, the quantitative elemental analysis was executed with X-ray fluorescence spectroscopy (XRF). The test portion was obtained by scooping the ash from the bag. It was first dried at 110 °C and then ignited at 950 °C. If necessary, the test portion was ground and sieved through a 0.090 mm sieve. The powder thus obtained was mixed with lithium–tetraborate, serving as a flux, in a 1:10 ratio. The mixture was fused at 1100 °C to create beads. These were analyzed with the *Bruker Tiger S8—4 kW* wavelength dispersive X-ray fluorescence spectrometer and the *Geomaj-Quant* program.

The quantity of free CaO was determined with the method specified in standard EN 451-1 [32]. A portion of ~20 g of material was sieved on a 63 µm sieve, and the residue was ground by mortar and pestle until it passed through the sieve. A homogenized portion of ~1.0–1.5 g was placed into a 250 mL flask and mixed with 12 mL of butanoic acid and 80 mL of butan-2-ol. The flask was fitted with the spiral reflux condenser and absorption tube and boiled for 3 h. The warm dispersion was filtered, and the residue was washed with 50 mL propan-2-ol. A few drops of bromophenol blue indicator were added to the filtrate and titrated with hydrochloric acid until the color changed to yellow. The free CaO content was calculated from the volume of titrant and expressed as wt% of the dry portion of tested ash.

In terms of the cement and concrete industry, soundness refers to the reactivity of free lime, magnesia, and excess sulfates in cementitious materials. These reactions are expansive and may cause cracking in young concrete. The soundness is normally determined with the Le Chatelier method, detailed in EN 196-3 [33] standard. The test specimen was prepared according to EN 450-1 [34] by first blending 70 wt% of cement with 30 wt% of OSA and then adding a sufficient amount of water to form a paste of standard consistency. The paste was placed in the Le Chatelier mold and stored at $\geq$90 % relative humidity at 20 $\pm$ 1 °C for 24 h when the initial distance between the needles was measured. The mold was then placed in a water bath and boiled for 3 h. The molds were then removed from the bath and left to cool to room temperature whereupon the final distance between the needles was determined and the difference between the final and initial distance was calculated.

The chemical reactivity was assessed with isothermal calorimetry following the procedure suitable for the SCMs. The procedure specified in the ASTM C1897-20 [35] standard detects hydraulic and pozzolanic reactions, which are exothermic by nature. Thus, the amount of released heat is the measure of reactivity. One specimen of 10.00 g was used

for the analysis. It was collected from the bag by scooping. The specimen was combined with 30.00 g of calcium hydroxide, 5.00 g of calcium carbonate, and 54.00 g of potassium solution and mixed for 3 min to obtain a smooth paste. A test portion of 15 ± 0.01 g of the paste was placed into a glass ampoule. The ampule was inserted into the *TA Instruments calorimeter TAM Air 8*, where distilled water was used as the reference material. The measurements were conducted over seven days at a temperature of 40 °C. The cumulative heat of hydration H_{SCM} (J kg^{-1}) stated as heat released per unit mass of SCM in the test portion was calculated.

2.3.3. Mineralogical Characteristics

The qualitative phase analysis, which gives an overall insight into the mineralogical composition, was performed by X-ray Diffraction (XRD). The test portions were obtained by quartering the received samples to a suitable amount, which was dried in an oven at 60 °C to a constant mass. A portion of 100 g of material was ground with a disc mill to a particle size < 500 μm. The quartering of the material was repeated, and a suitable quantity was ground in an agate mortar to a particle size of <63 μm. The test portion was placed into a 27 mm diameter sample holder for analysis.

The analysis was performed on the *Panalytical Malvern Empyrean* diffractometer with Cu–Kα radiation. The measurements were carried out at laboratory temperature. The tube voltage was set to 45 kV and current to 40 mA. Data were collected over the 2θ range from 5 to 70° in increments of 0.013°. The increment measurement time was 150 s. The results were analyzed with *Panalytical Highscore 4.8* diffraction software using the *ICDD Powder Diffraction File PDF-4+* database as a source of references for the crystalline phases.

2.4. Characterization of Printable Concrete

The performance of OSA in concrete formulations for 3D printing was assessed in three stages. In the first stage, the formulations containing OSA were adjusted to the same workability as the reference formulation. Secondly, the mechanical tests were conducted on all formulations, and in the third stage, the reference formulation and two OSA formulations with the best mechanical performance were selected for printability tests.

In terms of dry components, the formulations consisted of 33 wt% of powder and 67 wt% of sand. In the reference formulation, the powder contained only cement, while in OSA formulations, it was split into 10 wt% of ash and 23 wt% of cement [34,36]. A superplasticizer in the amount of 1 wt% of mass of water was also added. The following types of materials were used: cement CEM I 42.5N from *Schwenk Ltd.* (Brocēni, Latvia), sand 0/2 mm from *Sakret Ltd.* (Rumbula, Latvia), and superplasticizer *Floormix* from *Vincents Polyline Ltd.* (Kalngale, Latvia).

The workability of OSA formulations was adjusted according to EN 450-1 [34] to maintain the same consistency for all formulations. The consistency was confirmed with the flow table method specified in EN 1015-3 [37]. A sufficient amount of water containing 1 wt% of superplasticizer was added so that OSA formulations were within the ±10 mm range of the reference, whose spread after 25 jolts was 180 mm. The reference formulation was known to be printable from previous printing tests. Proportions of the components in tested concrete formulations are given in Table 3.

Table 3. Composition of concrete formulations expressed as mass per 1000 g of dry components. Superplasticizer was added in the amount of 1 wt% of mass of water, and water was adjusted to retain the consistency in the range of ±10 mm of the reference formulation measured on the flow table. Notation: ash: OSA—oil shale ash, OSWA—oil shale + wood ash; power plants: Ees—*Eesti*, Ene—*Enefit280*, and Auv—*Auvere*; ash extraction method: nid—novel integrated desulfurizer, ef—electrostatic filters, ba—bottom ash; collision milling frequency on a *Desi-11* disintegrator: 50, 100, 130 Hz.

Ash and Concrete Formulation Designation	Mass of Components per 1000 g of Dry Materials (g)				
	Ash	Cement	Sand	Water	Superplasticizer
Ref	---	333.3	666.7	141.7	1.42
OSA-Ees(nid)	100.0	233.3	666.7	146.7	1.47
OSA-Ees(nid)/100	100.0	233.3	666.7	143.3	1.43
OSA-Ene(ef)	100.0	233.3	666.7	166.7	1.67
OSA-Ene(ef)/100	100.0	233.3	666.7	160.0	1.60
OSWA-Auv(ef)	100.0	233.3	666.7	186.7	1.87
OSWA-Auv(ef)/100	100.0	233.3	666.7	173.3	1.73
OSWA-Auv(ba)/<1 mm *	100.0	233.3	666.7	160.6	1.61
OSWA-Auv(ba)/50	100.0	233.3	666.7	156.1	1.56
OSWA-Auv(ba)/100	100.0	233.3	666.7	147.7	1.48
OSWA-Auv(ba)/130	100.0	233.3	666.7	148.1	1.48

* The bottom ash in its original form was too coarse to be used as cement replacement; thus, only the portion passing through the 1 mm sieve was used.

The choice of fixing the spread by adjusting the water and superplasticizer content was made because printability is the principal parameter in this study. As a result, the water–powder ratio is not fixed, which may have a bearing on the mechanical properties. However, printable formulations need to be cohesive, and to achieve this, a high powder content with a sufficient amount of water to wet the particles is required. The water requirement depends on particle size, morphology, texture, and mineralogical composition.

2.4.1. Mechanical Properties

The mechanical characteristics of printable concrete mixtures containing unprocessed and milled ash were assessed with compressive and flexural strength tests 7, 28, and 56 days after casting the specimens. The specimens for compression tests were cubes with nominal dimensions of 20 mm, while specimens for the flexural test were prisms with nominal dimensions $b \times h \times L$ of $40 \times 40 \times 160$ mm^3. The preparation and curing of the specimens were carried out according to EN 1015-11 [38]. The specimens were demolded ~24 h after casting and kept in a storage chamber at a relative humidity of 95 ± 5 % and a temperature of 20 ± 2 °C until the time of the test. The tests were carried out on the *Controls 50-C56Z00* machine in a force-controlled mode at a stress rate of 0.8 MPa s^{-1} for compression tests and in a displacement-controlled mode at 0.5 mm s^{-1} for the flexural tests.

2.4.2. Printability Assessment

Two formulations exhibiting the best mechanical performance, namely, OSA-Ees(nid) and OSA-Ees(nid)/100, were selected for printability assessment, which was carried out with the slug test and direct buildability test. Both tests were performed on the custom-made gantry-type laboratory concrete printer located at RTU and shown in Figure 3. Its print area dimensions are 1500×1000 m^2, while the clearance is 1 m. The printhead comprises a hopper of 15 L from where the material is pushed through the nozzle by means of a helix screw conveyor. The nozzle of a circular cross-section with a diameter of 25 mm was used, and the material flow was regulated to form a 40–45 mm wide filament at a pre-selected layer height of 10 mm.

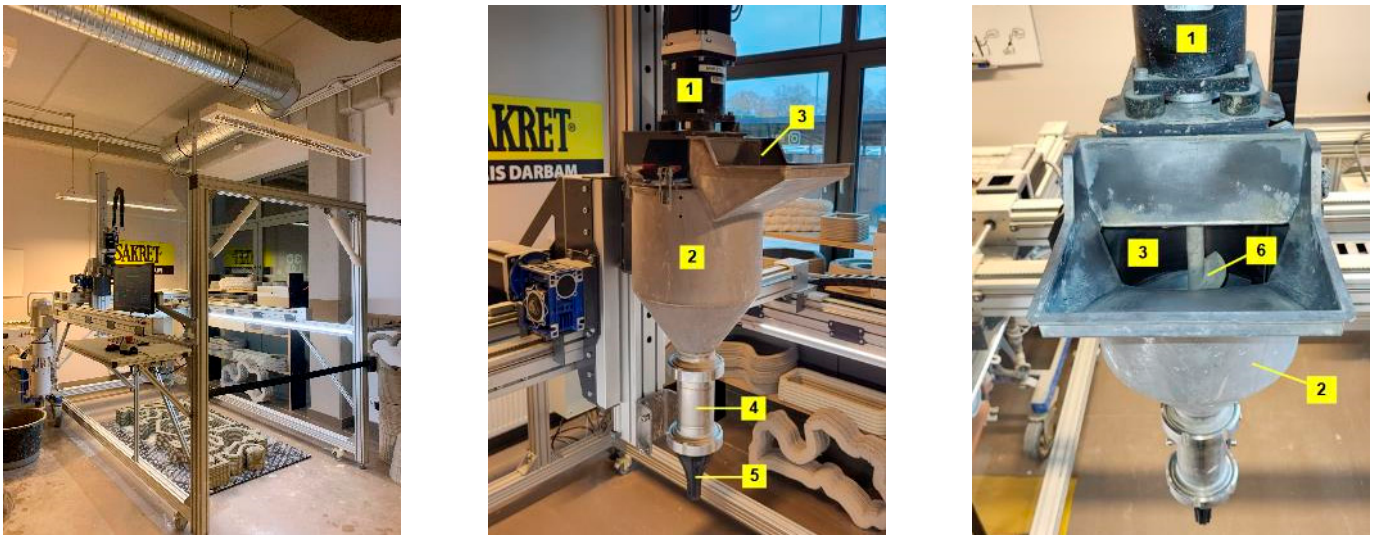

(**a**) (**b**) (**c**)

Figure 3. Custom-made laboratory concrete printer at *Riga Technical University* (RTU): (**a**) the printer set up with the aluminum frame and print area; (**b**) the printhead closeup; and (**c**) the hopper. Labeled parts: 1—motor; 2—hopper, 3—inlet; 4—pipe; 5—nozzle; and 6— helix screw conveyor.

The slug test was performed according to the method proposed by Ducoulombier et al. [39] where the material is extruded under a constant force through the printer's nozzle. The nozzle is positioned vertically ~50 cm above the print area, and the extruded filament breaks as a result of uniaxial yielding, thus forming a droplet or a slug. Once a uniform flow is achieved, 25 slugs are collected in a container, and their cumulative mass is measured. The yield stress τ_y (Pa) is determined as per Equation (1)

$$\tau_y = m_s \frac{g}{S\sqrt{3}}\,, \tag{1}$$

where m_s (kg) is the average mass of a slug, g (m s^{-2}) is gravity, and S (m^2) is the nozzle cross-section.

The direct buildability test was performed immediately after the slugs test by printing a cylinder with a diameter of 250 mm until plastic collapse occurred [40]. The lap time needed for a single layer to print was ~4 s, resulting in a total printing time of ~1 min. Therefore, the mixture was extruded ~16–17 min after water was added to dry components. The compressive stress at plastic collapse σ_p (Pa) and yield stress τ_y (Pa) are calculated according to Equations (2) and (3) [41], respectively

$$\sigma_p = \rho\, n\, h\, g\,, \tag{2}$$

$$\tau_p = \frac{\rho\, n\, h\, g}{\sqrt{3}} \tag{3}$$

where ρ (kg m^{-3}) is density, n (1) is the number of layers at the time of collapse, and h (m) is the height of the layer. Additionally, the surface quality was visually checked, and the printed cylinder was measured to assess the dimensional consistency of the filament width.

Before commencing the printability tests and 15 min after adding water to the dry components, the density of the fresh mixture was determined according to EN 12350-6 [42]. It was measured by filling a 1 L container in two layers, compacting each layer 25 times using a compacting rod, leveling the top surface with a trowel, and then weighing the container.

3. Results

This chapter presents and discusses the results in relation to the test method. The results are coupled in Chapter 4 where the discussion pertaining to the individual type of ash is given.

3.1. Properties of OSA

Moisture content was determined to find if a noteworthy amount of moisture is absorbed during pretreatment, as it may cause hydration reactions that impact the mineralogical composition. It is observed in Table 4 that moisture content is negligible. The particle density values, also collated in Table 4, are somewhat higher than values normally observed on fly ash from coal-burning power plants, which are between 2.2 and 2.5 kg L^{-1}, and somewhat lower than values found in cement, those normally standing at ~3 kg L^{-1}. The particle density values are needed in the concrete mix design process.

Table 4. Moisture content and particle density measured on ash milled at 100 Hz. Notation: ash: OSA—oil shale ash, OSWA—oil shale + wood ash; power plants: Ees—*Eesti*, Ene—*Enefit280*, and Auv—*Auvere*; ash extraction method: nid—novel integrated desulfurizer, ef—electrostatic filters, ba—bottom ash; collision milling frequency on a *Desi-11* disintegrator: 100 Hz.

	Moisture Content (wt%)	**Particle Density (kg L^{-1})**
OSA-Ees(nid)/100	0.7	2.6130 ± 0.002
OSA-Ene(ef)/100	0.9	2.7504 ± 0.004
OSWA-Auv(ef)/100	0.4	2.6825 ± 0.003
OSWA-Auv(ba)/100	0	2.6862 ± 0.004

The PSDs of OSA before and after pretreatment with collision milling are collated in Figure 4 as differential passing curves and in Figure 5 as 50 and 95 wt% demarcation diameters. The latter is the diameter at which either 50 or 95 wt% of the particles are smaller than the stated value. The results for cement CEM I are added for comparison. Out of the three types of fly ash, namely, OSA-Ees(nid), OSA-Ene(ef), and OSWA-Auv(ef), the first one is the finest with the peak in differential particle size curve at ~6 μm, while the latter two peak between ~30 and 50 μm. When comparing these three types of ash to their milled counterparts, namely, OSA-Ees(nid)/100, OSA-Ene(ef)/100, and OSWA-Auv(ef)/100, the differential curves indicate that collision milling at 100 Hz predominantly reduces particles larger than 10 μm so that in case of the latter two, the peak is shifted to between ~10 and 20 μm. In the case of OSA-Ees(nid)/100, the peak remains at ~6 μm; however, the percentage passing increases from ~6 to ~8 wt%. This is also reflected in the demarcation diameter of OSA-Ees(nid)/100. Namely, the 50 wt% demarcation diameter remains approximately the same at 8–9 μm, whereas the 95 wt% one is reduced from 100 to 40 μm. Comparison to CEM I shows that OSA-Ees(nid) is finer than cement already in its original condition, while in the case of OSA-Ene(ef) and OSWA-Auv(ef), collision milling at 100 Hz reduces the particles closer to the CEM I distribution.

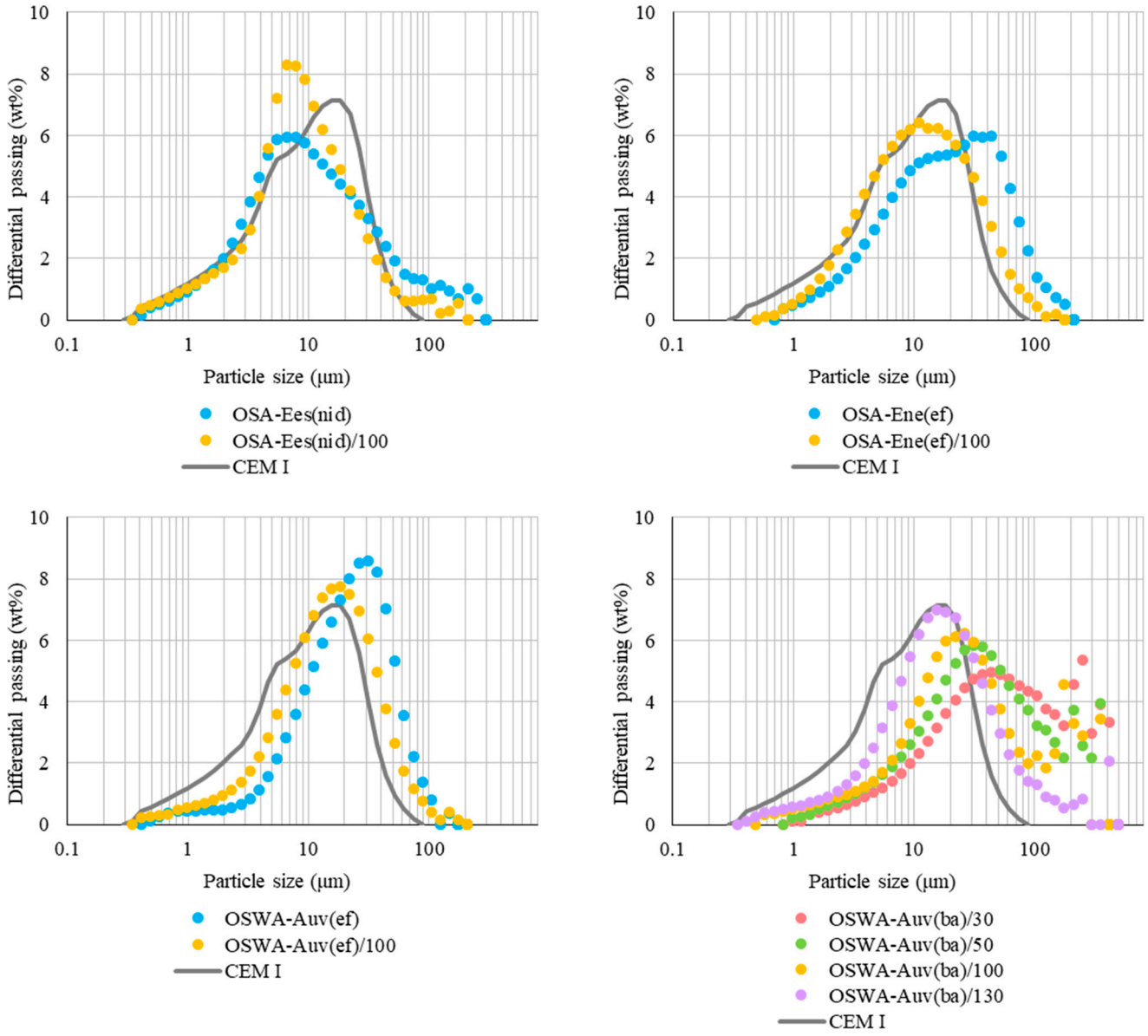

Figure 4. Particle size distribution (PSD) of ash before and after collision milling measured with laser diffraction. For comparison purposes, the PSD of CEM I 42.5N from *Schwenk Ltd.* (Brocēni, Latvia) is also presented. Notation: ash: OSA—oil shale ash, OSWA—oil shale + wood ash; power plants: Ees—*Eesti*, Ene—*Enefit280*, and Auv—*Auvere*; ash extraction method: nid—novel integrated desulfurizer, ef—electrostatic filters, ba—bottom ash; collision milling frequency on a *Desi-11* disintegrator: 30, 50, 100, 130 Hz.

The OSWA-Auv(ba) ash, being collected at the bottom of the furnace, is too coarse for the laser diffraction analysis prior to milling. The curves, therefore, show the ash milled at 30, 50, 100, and 130 Hz. The peak of OSWA-Auv(ba)/30 was at ~50 μm, and with increased frequency, it moved to ~10 μm for OSWA-Auv(ba)/130. At the same time, the curve gradually narrowed so that the peak increased in height from ~5 to ~7 wt%. Similarly, the 50 wt% demarcation diameter decreased from ~50 to ~15 μm and the 95 wt% diameter from ~320 to ~130 μm. Therefore, as a result of collision milling, the PSD curve of OSWA-Auv(ba) gradually shifts closer to the PSD curve of CEM I as the milling frequency increases. Overall, it can, therefore, be concluded that collision milling is efficient for reducing the size of particles larger than 10 μm.

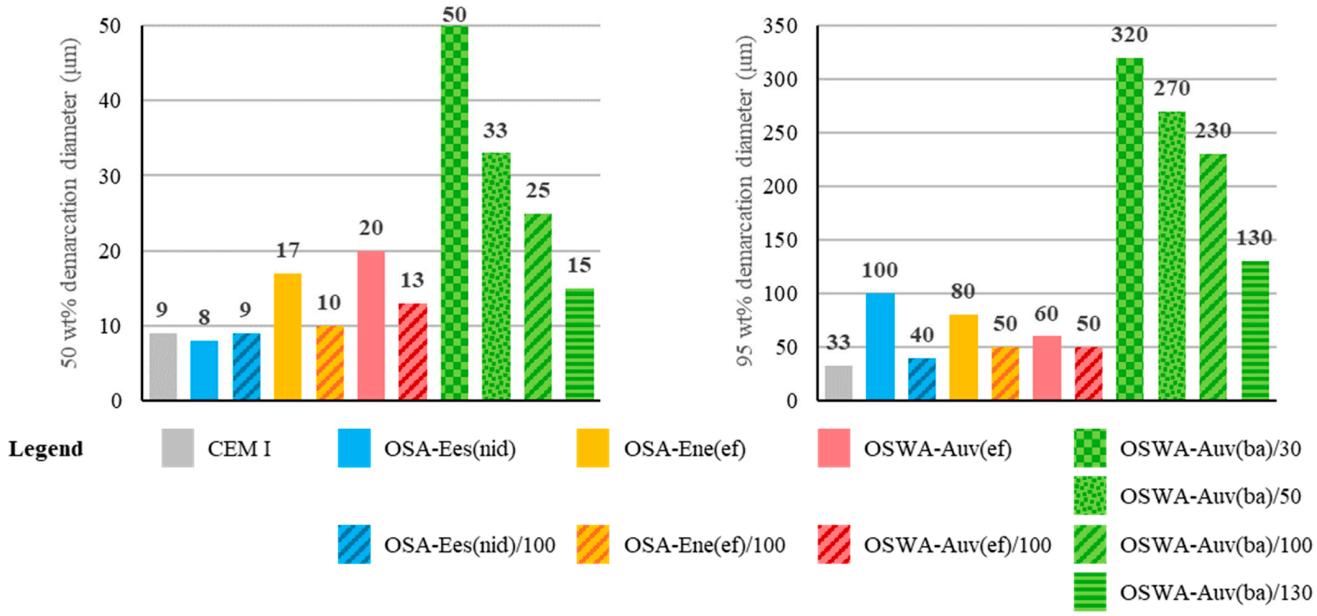

Figure 5. Demarcation diameter at which either 50 or 95 wt% of the particles are smaller than the stated value. For comparison purposes, the results for CEM I 42.5N from *Schwenk Ltd.* (Brocēni, Latvia) are also presented. Notation: ash: OSA—oil shale ash, OSWA—oil shale + wood ash; power plants: Ees—*Eesti*, Ene—*Enefit280*, and Auv—*Auvere*; ash extraction method: nid—novel integrated desulfurizer, ef—electrostatic filters, ba—bottom ash; collision milling frequency on a *Desi-11* disintegrator: 30, 50, 100, 130 Hz.

The results of SEM are summarized in Figures 6 and 7, where a heterogenic distribution of particles is observed in all types of ash. The particles that are similar to cenospheres found in fly ash from coal power plants, having a smooth surface and dimensions up to 30 µm, are abundant in OSA-Ees(nid), while in OSA-Ene(ef), only a few are found. The morphology of the two types of ash collected at the electrostatic filters, namely, OSA-Ene(ef) and OSWA-Auv(ef), is predominantly angular with a rather smooth texture.

The effect of pretreatment with collision milling on particle morphology and texture can be analyzed in Figure 6, where images of ash before and after milling at 100 Hz are lined up. Overall, it is observed that milling does not significantly affect the shape of the particles. Namely, the particles of OSA-Ene(ef) and OSWA-Auv(ef) are angular even before the milling, while in OSA-Ees(nid) it is mostly larger, angular particles that are crushed while milling does not reduce the size of the smaller spherical particles.

The impact of milling frequency can be studied in Figure 7, which lines up images of OSWA-Auv(ba) milled at 30, 50, 100, and 130 Hz. The particles of this type of ash are also angular, and no impact on morphology and texture is observed. However, it is clear that as frequency increases, the number of large particles decreases.

The elemental composition shown in Table 5 indicates that ash filtered from the flue gasses contains ~20–30 wt% of SiO_2 and ~30–40 wt% CaO, while the content of these two oxides in bottom ash is ~5 and ~50 wt%, respectively. Compared to the results of free CaO content collated in Table 6, it can be concluded that in these three types of ash, the majority of CaO is consumed for the formation of minerals, such as dicalcium silicate. Nevertheless, the requirement for the presence of free CaO in fly ash from coal-burning power plants set by EN 450-1 [34] is $\leq$1.5 wt%. Ash that exceeds this limit must be further tested for soundness, and the expansion measured between the tips of the Le Chatelier ring should be $\leq$10 mm. The soundness results in Table 6 show that all types of ash meet this requirement. The same standard also sets the limit for the total equivalent alkali content

at ≤5 wt%. The latter, calculated as (wt% Na_2O + 0.658 × wt% K_2O), is between ~1 and 3 wt%.

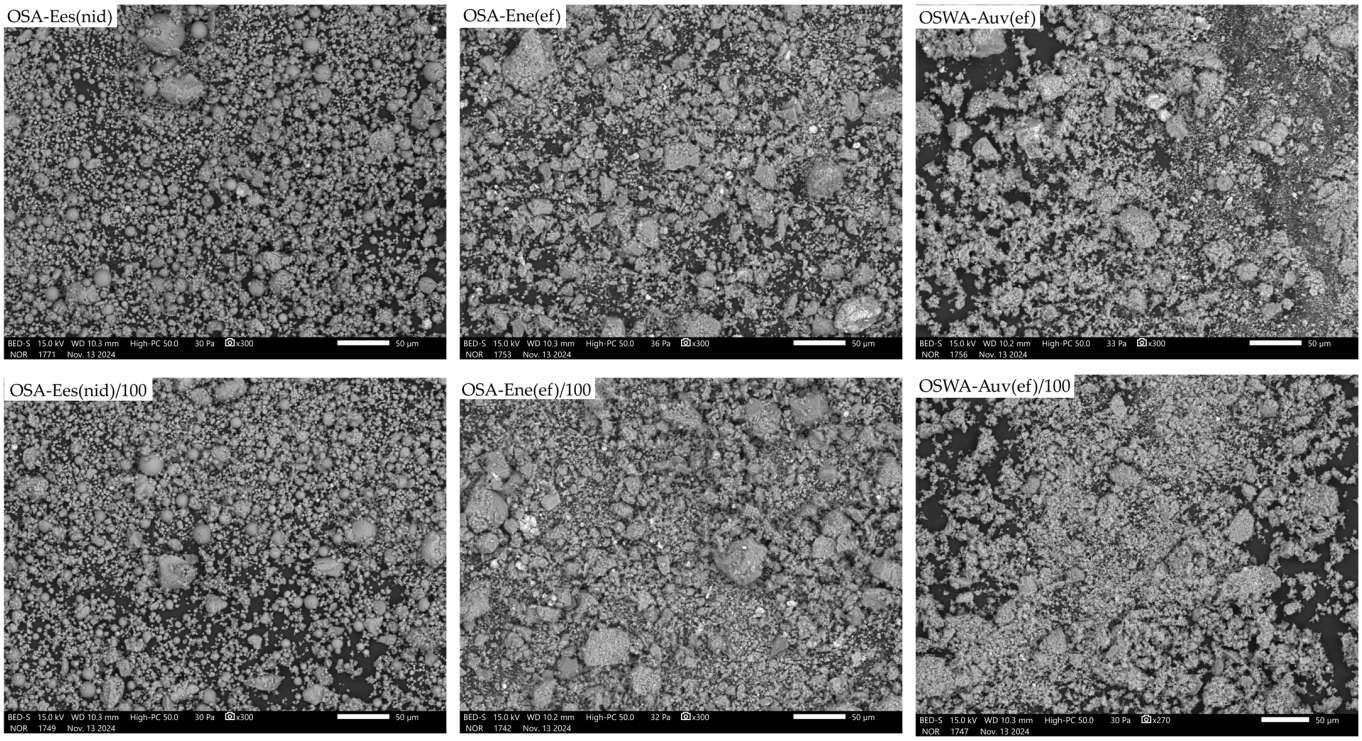

Figure 6. Scanning electron microscope (SEM) images of ash particles before (**top** row) and after collision milling (**bottom** row). Notation: ash: OSA—oil shale ash, OSWA—oil shale + wood ash; power plants: Ees—Eesti, Ene—Enefit280, and Auv—Auvere; ash extraction method: nid—novel integrated desulfurizer, ef—electrostatic filters; collision milling frequency on a Desi-11 disintegrator: 100 Hz.

The LOI, in principle, originates either from the dehydration and decomposition of minerals or from unburnt organic matter, such as hydrocarbons. The LOI limit set by EN 450-1 [34] is ≤9 wt%, and in comparison, the values obtained on OSA-Ene(ef), OSWA-Auv(ef), and OSWA-Auv(ba) of ~20–30 wt% are high. This indicates a possibility that they still contain a significant amount of kerogen, a complex mixture of hydrocarbon compounds that is a primary organic component of oil shale. However, decomposition is a complex process that depends on the mineralogy of oil shale and the thermal maturity of kerogen [43], and in order to identify the decomposing constituents, further analysis with thermogravimetry (TG) coupled with Fourier-transform infrared spectroscopy (FTIR) is needed.

The results of isothermal calorimetry are summarized in Figure 8. The chemical reactivity is assessed as the cumulative heat released due to the exothermic reactions. The three types of flue gas ash, namely, OSA-Ees(nid), OSA-Ene(ef), and OSWA-Auv(ef), exhibit low chemical reactivity before milling as the cumulative heat is between ~10 and 20 J g^{-1}. Collision milling at 100 Hz results in a more than seven-fold increase in reactivity, with a cumulative heat release of ~100–150 J g^{-1} found in OSA-Ees(nid)/100, OSA-Ene(ef)/100, and OSWA-Auv(ef)/100. For comparison, fly ash, certified for use in concrete, released ~70 J g^{-1} after 200 h. There are two possible causes for increased reactivity due to milling, firstly, the smaller the particles, the larger the surface area in contact with water, and secondly, reactive phases in the kernel may be coated by a shell of inert phases—as milling breaks the inert shell, the reactive kernel becomes exposed.

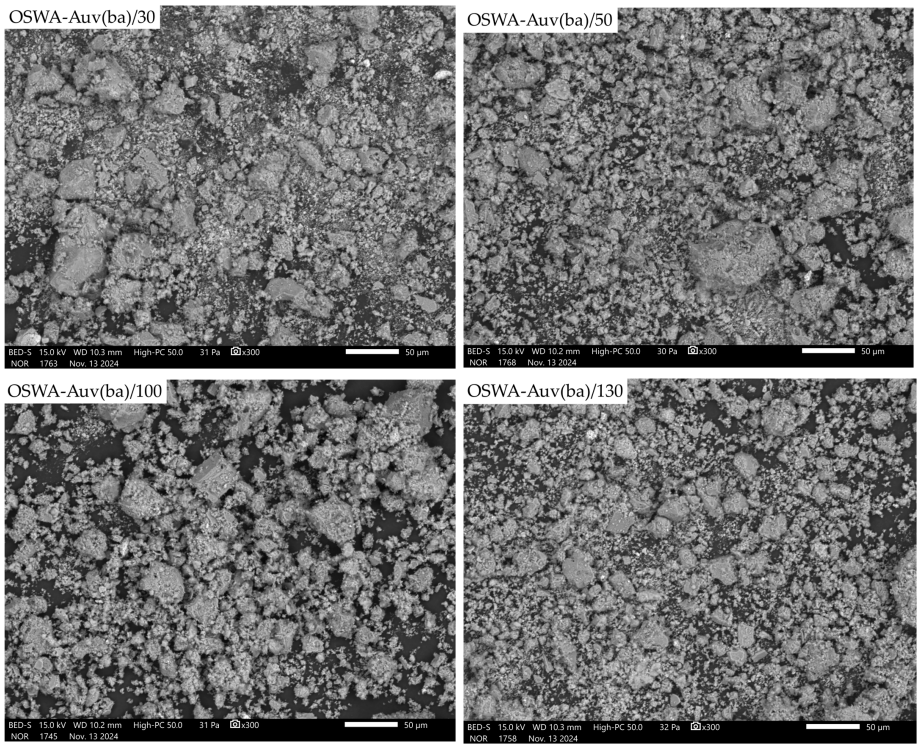

Figure 7. Scanning electron microscope (SEM) images of ash particles. Notation: ash OSWA—oil shale + wood ash; power plant: Auv—*Auvere*; ash extraction method: ba—bottom ash; collision milling frequency on a *Desi-11* disintegrator: 30, 50, 100, 130 Hz.

Table 5. Elemental composition measured with X-ray fluorescence spectroscopy (XRF) and loss on ignition (LOI). Notation: ash: OSA—oil shale ash, OSWA—oil shale + wood ash; power plants: Ees—*Eesti*, Ene—*Enefit280,* and Auv—*Auvere*; ash extraction method: nid—novel integrated desulfurizer, ef—electrostatic filters, ba—bottom ash.

Ash Designation	Composition (wt%)											
	SiO_2	Al_2O_3	Fe_2O_3	CaO	MgO	SO_3	Na_2O	K_2O	Mn_2O_3	TiO_2	P_2O_5	LOI
OSA-Ees(nid)	21.5	5.6	2.9	35.6	3.0	17.3	0.4	2.9	<0.1	0.3	0.1	9.6
OSA-Ene(ef)	28.0	6.9	4.0	29.5	3.0	4.9	0.1	3.4	<0.1	0.4	0.1	19.1
OSWA-Auv(ef)	22.2	5.5	3.7	41.8	3.4	4.9	<0.1	2.8	<0.1	0.3	0.2	14.4
OSWA-Auv(ba)	6.0	1.4	2.5	50.8	2.3	3.1	0.1	0.6	<0.1	0.1	0.1	32.9

Table 6. Free lime content measured with hydrochloric acid titration and the soundness of ash determined with the Le Chatelier method. Notation: ash: OSA—oil shale ash, OSWA—oil shale + wood ash; power plants: Ees—*Eesti*, Ene—*Enefit280,* and Auv—*Auvere*; ash extraction method: nid—novel integrated desulfurizer, ef—electrostatic filters, ba—bottom ash.

Ash Designation	Free CaO (wt%)	Soundness (mm)
OSA-Ees(nid)	4.5	3.6
OSA-Ene(ef)	<0.1	2.3
OSWA-Auv(ef)	21.8	2.0
OSWA-Auv(ba)	8.1	0.9

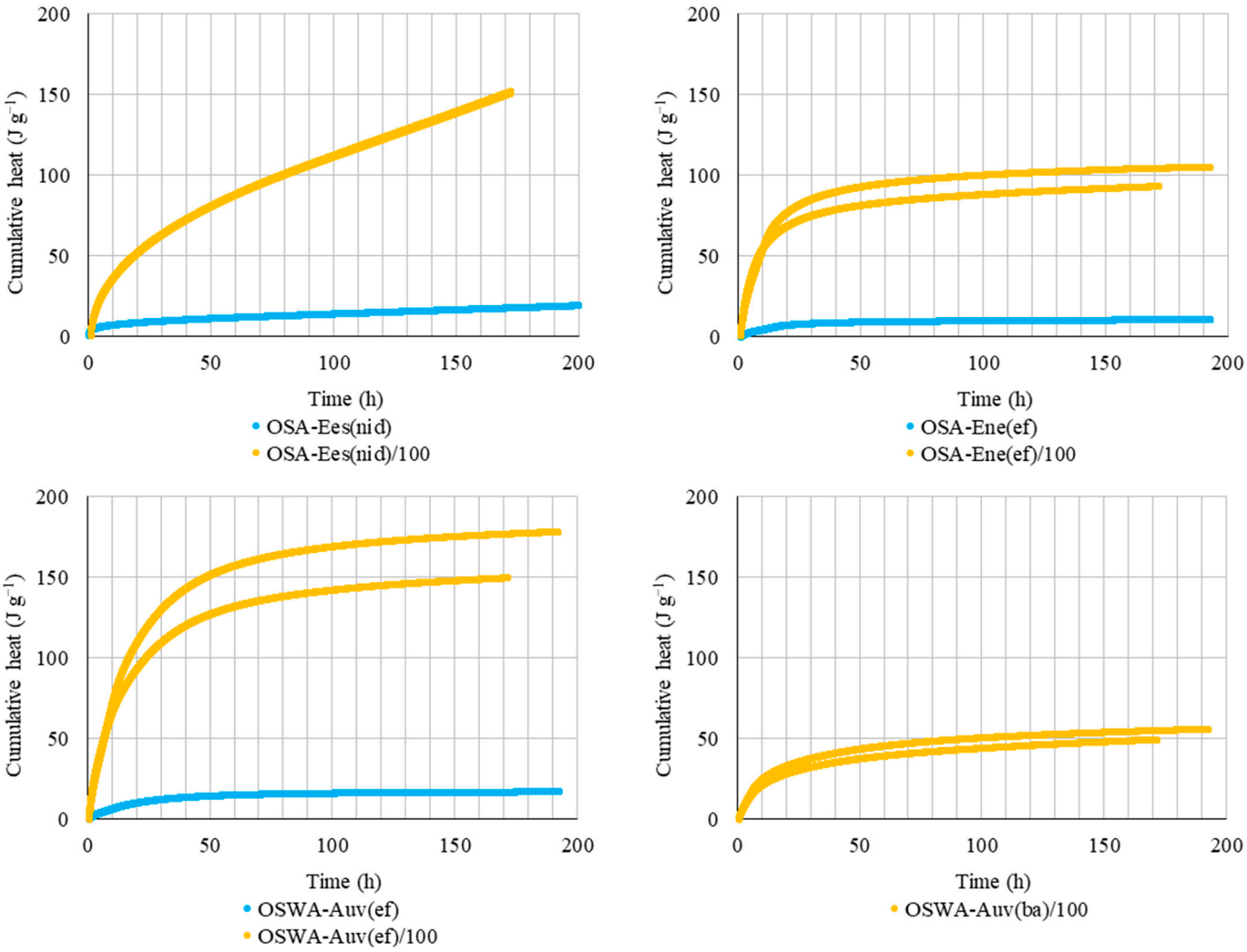

Figure 8. Chemical reactivity determined by isothermal calorimetry. Notation: ash: OSA—oil shale ash, OSWA—oil shale + wood ash; power plants: Ees—*Eesti*, Ene—*Enefit280*, and Auv—*Auvere*; ash extraction method: nid—novel integrated desulfurizer, ef—electrostatic filters, ba—bottom ash; collision milling frequency on a *Desi-11* disintegrator: 100 Hz.

The reactivity of OSWA-Auv(ba) was measured only on ash collision milled at 100 Hz since unmilled ash is too coarse for the isothermal calorimetry test. In comparison to the three types of milled fly ash, the milled bottom ash exhibits two to three times lower reactivity with a cumulative heat of ~50 J g^{-1}.

The results of the qualitative XRD phase analysis are summarized in Table 7. XRD phase analysis established that all the investigated types of ash contained calcite, quartz, and anhydrite. The reactive β-dicalcium silicate (larnite) was found in all samples, except for OSWA-Auv(ba). Its γ polymorph was identified in OSA-Ees(nid) and OSWA-Auv(ef), suggesting that during cooling, part of the β modification transformed to the γ polymorph. Calcite is most abundant in OSWA-Auv(ba), while its quantity is the lowest in OSWA-Auv(ef) and OSA-Ees(nid).

Table 7. Mineralogical composition established with X-ray diffraction (XRD) where a dot (•) marks the presence of a mineral. Notation: ash: OSA—oil shale ash, OSWA—oil shale + wood ash; power plants: Ees—*Eesti*, Ene—*Enefit280*, and Auv—*Auvere*; ash extraction method: nid—novel integrated desulfurizer, ef—electrostatic filters, ba—bottom ash.

Ash Designation	Anhydrite	β-Dicalcium Silicate	Calcite	γ-Dicalcium Silicate	Dolomite	Feldspar	Hematite	Lime	Mellilite	Muscovite	Periclase	Portlandite	Quartz	Rokühnite	Spinel	Sylvite
OSA-Ees(nid)	•	•	•	•				•			•	•	•	•	•	•
OSA-Ene(ef)	•	•	•		•	•	•		•	•			•			
OSWA-Auv(ef)	•	•	•	•		•	•	•	•		•	•	•			
OSWA-Auv(ba)	•		•		•			•	•			•	•			•

Lime content was the highest in OSWA-Auv(ef), and smaller amounts were also found in OSA-Ees(nid) and OSWA-Auv(ba). In OSA-Ene(ef), all lime and portlandite are fully hydrated and carbonated to form calcite. The highest amount of portlandite was detected in OSA-Ees(nid), whereas in the other ashes, portlandite was already transformed into calcite. Sulfate, present as anhydrite, was found in all ashes. In OSA-Ees(nid) and OSWA-Auv(ef), anhydrite was more abundant compared to OSWA-Auv(ba). Chlorine-bearing phases, such as sylvite, were identified in OSA-Ees(nid) and OSWA-Auv(ba). Additionally, a Fe-bearing chlorine phase was detected in OSA-Ees(nid).

3.2. Properties of Printable Concrete Containing OSA

The results of the compression and flexural tests conducted on the reference formulation and formulations with OSA are summarized in Figure 9. Generally, it is expected that replacing cement with OSA shall result in reduced strength, and, overall, this stipulation is confirmed. The 56-day compressive and flexural strength of the reference formulation was ~60 and ~7.5 MPa, respectively. With the exception of OSA-Ees(nid), these values were between ~30–45 and ~6.0–7.0 MPa, respectively, for ash-containing formulations. The OSA-Ees(nid) formulation, on the other hand, exhibits a similar strength range as the reference, especially when the intersample variability observed on two reference sample groups is taken into account. In terms of early strength, the results indicate that after 7 days, the reference and the OSA-Ees(nid) formulation reach ~60% of 56-day compressive strength, while for the other ash-containing formulations, this value is ~70%. Considering the intra- and intersample variability, it can be concluded that neither of the tested formulations exhibits any significant strength gain after 28 days.

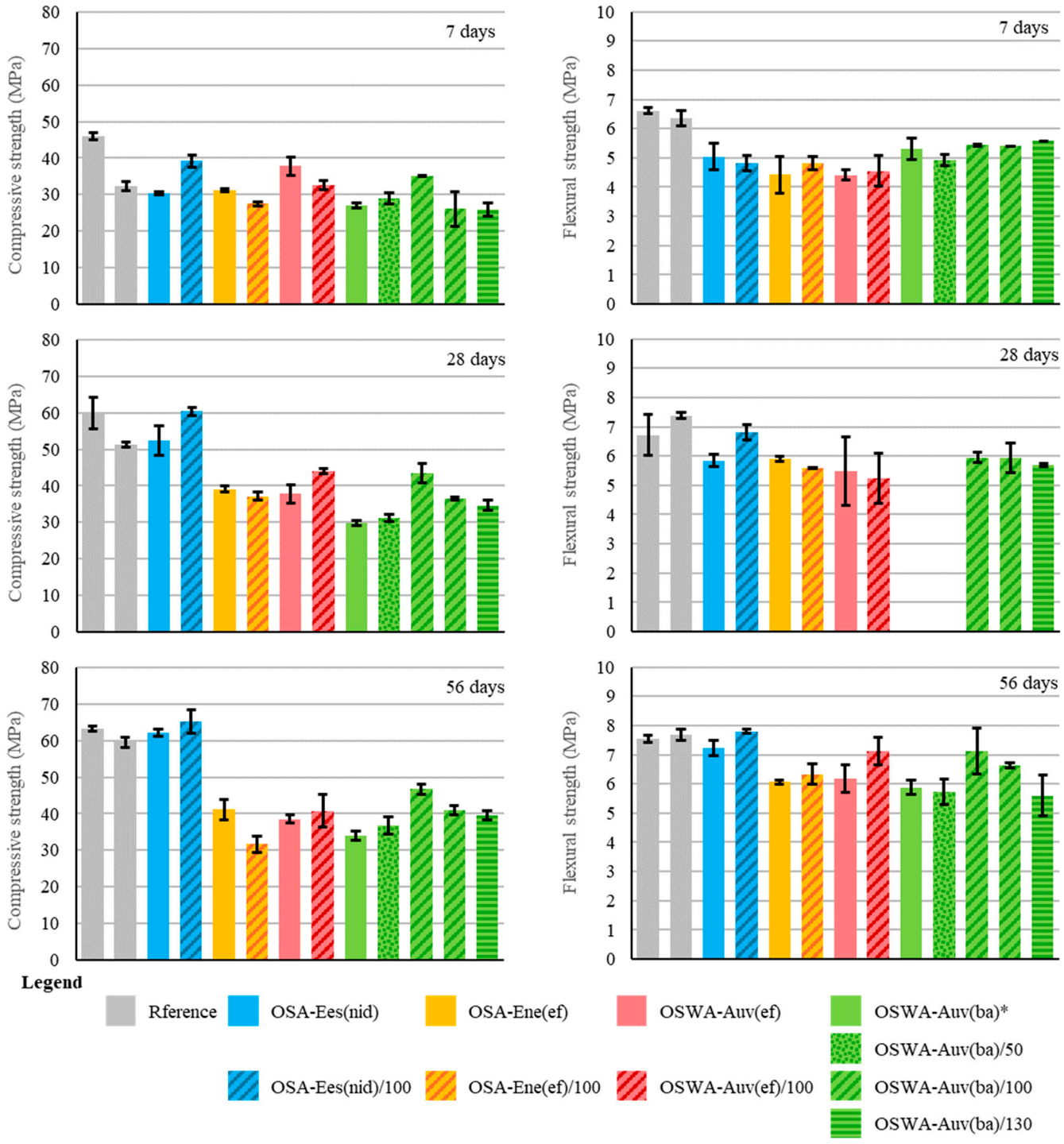

Figure 9. Compressive and flexural strength of printable concrete 7, 28, and 56 days after casting. Notation: ash: OSA—oil shale ash, OSWA—oil shale + wood ash; power plants: Ees—*Eesti*, Ene—*Enefit280*, and Auv—*Auvere*; ash extraction method: nid—novel integrated desulfurizer, ef—electrostatic filters, ba—bottom ash; collision milling frequency on a *Desi-11* disintegrator: 50, 100, 130 Hz; *—ash in original form was too coarse to be used without processing; thus, portion passing through a 1 mm sieve was used.

The compression test results obtained on the OSWA-Auv(ba) series consistently show strength gain when milling frequency increases from 50 to 100 Hz, whereas further frequency increase causes strength drop. Nevertheless, overall, it may be concluded that formulations with milled bottom ash performed better than those with unmilled fine bottom ash (sieved fraction of < 1 mm). This indicates that bottom ash, usually unsuitable for

direct cement replacement due to its large particle size, may become a viable SCM after pretreatment with collision milling, which is most effective at around 100 Hz.

Overall, it may be concluded that collision milling of OSA enhances the mechanical properties of ash-containing concrete formulations, although the effectiveness varies by the type of ash. Neither the PSD nor the chemical reactivity of the ash is in a direct correlation with strength as far as the results of this study are concerned; however, the results pool is not sufficient to draw firm conclusions.

Based on the mechanical test results, two ash-containing formulations, namely, OSA-Ees(nid) and OSA-Ees(nid)/100, were selected for the printability assessment tests. The results, including the reference formulation, are collated in Table 8. These results show that the density of the reference and OSA-Ees(nid) formulation does not differ significantly (~15 g per 1 L of material), whereas the difference is more pronounced for OSA-Ees(nid)/100 (~100 g per 1 L of material). Since the milling of this ash increased the proportion of particles around the 10 μm mark, it may have improved particle packing.

Table 8. Properties measured on fresh concrete mixtures for printability assessment. Values for density, yield stress, and compressive stress at plastic collapse are rounded to the nearest 5. Notation: ash: OSA—oil shale ash; power plant: Ees—*Eesti*; ash extraction method: nid—novel integrated desulfurizer; collision milling frequency on a *Desi-11* disintegrator: 100 Hz.

Ash Designation	Density (kg m^{-3})	Slug Test	Buildability Test—Values at Plastic Collapse		
		Yield Stress τ_y (Pa)	Number of Layers	Compression Stress σ_y (Pa)	Yield Stress τ_y (Pa)
Reference	2140	1005	15	3150	1820
OSA-Ees(nid)	2125	1020	12	2500	1440
OSA-Ees(nid)/100	2230	1180	13	2840	1670

The yield stress measured with the slug test, despite being somewhat higher in the OSA-Ees(nid)/100 formulation (see Table 8), is in fact in a rather narrow range compared to the results reported by Ducoulombier et al. [39], who recorded values between ~250 and 1500 Pa. The buildability results show that the addition of ash reduces the number of layers at which the plastic collapse occurs. Comparing the yield stress results from the slug test to the results obtained in the buildability test, we find that the latter are consistently higher, which may be related to the time elapsed between the two tests. Yield stress from the buildability test is 1.8 times higher than observed in the slug test in the case of the reference formulation, while for the two ash formulations, this factor amounts to 1.4. These results may imply that the behavior of the reference formulation is more susceptible to elapsed time, and while its buildability is better than in the two ash formulations, pumpability might be impaired. This observation, however, requires further investigation.

Figure 10 shows the printed cylinders before and after the plastic collapse. Visual inspection reveals a small degree of tears in the filament of all three formulations. These were observed to be limited to the surface and not detrimental to the buildability. Adjustments to the extrusion rate and/or the speed of the printhead could fix the issue for these formulations, while fine tuning the composition is a matter of further investigation.

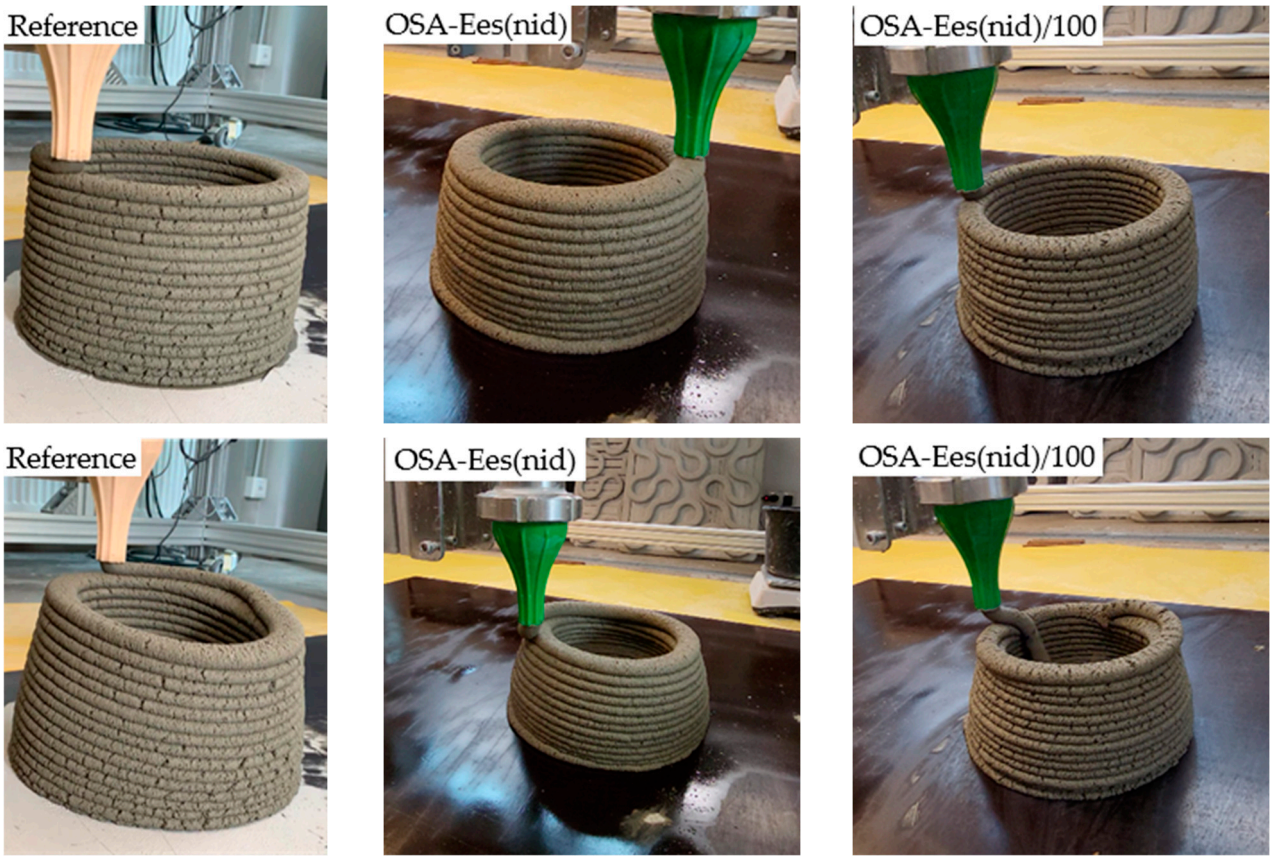

Figure 10. Direct buildability test showing printed objects before (**top** row) and after plastic collapse (**bottom** row). Notation: ash: OSA—oil shale ash; power plant: Ees—Eesti; ash extraction method: nid—novel integrated desulfurizer; collision milling frequency on a Desi-11 disintegrator: 100 Hz.

4. Discussion

OSA-Ees(nid), which is extracted from the flue gasses by the novel integrated desulfurizer, has the finest particles, with more than 50 wt% of them being smaller than 10 µm. This ash is the only one out of the four analyzed types of ash whose particles are mostly globular with a smooth surface. This ash contains ~35 wt% of CaO and ~20 wt% of SiO_2, which, as found in mineralogical analysis, form dicalcium silicate (C_2S). C_2S is present as β and γ polymorphs, with β being the reactive form and γ a rather inert form [44], which most likely precipitated from the β polymorph during cooling. The β polymorph of dicalcium silicate is also one of the principal minerals found in cement. On the other hand, ~5 wt% of CaO is found in a free form, but it does not cause an excessive expansion, which was tested with the soundness test. Furthermore, the equivalent alkali content and LOI are both within limits otherwise set for fly ash from coal power plants. Overall, these characteristics indicate that OSA-Ees(nid) could be suitable for use in concrete.

The reactivity of OSA-Ees(nid) measured with the isothermal calorimetry is, nevertheless low, with only ~20 J g^{-1} of released heat. While collision milling increased the released heat to ~150 J g^{-1}, this was not transformed into a significant improvement in mechanical properties. Namely, the 56-day compressive and flexural strength was found to be ~60 and ~7.5 MPa, respectively, for both OSA-Ees(nid) and OSA-Ees(nid)/100. These results, however, are approximately the same as measured on the reference concrete formulation. The printability of concrete formulations containing either milled or unmilled ash was also very similar. Hence, it should be concluded that while OSA-Ees(nid) is the most suitable ash out of the four tested, collision milling does not significantly improve its performance as an SCM, and such pretreatment is not likely to be viable.

The most significant impact of collision milling is observed in bottom ash OSWA-Auv(ba). In its original form, its particles are up to 2 cm big, and reducing the particle size is necessary to consider this ash as a potential SCM. Increasing the milling frequency from 30 to 130 Hz results in a decrease in average particle size, with a 50 wt% demarcation diameter being ~50 μm at 30 Hz and 15 μm at 130 Hz. The optimal frequency, however, appears to be ~100 Hz since the concrete formulation containing OSWA-Auv(ba)/100 exhibits the highest strength. Nevertheless, despite milling at 100 Hz, the reactivity of OSWA-Auv(ba) remains low with the cumulative heat release of ~50 J g^{-1}. This is probably related to the absence of any C_2S phases. On one hand, the SiO_2 content of ~5 wt% is low compared to ~50 wt% of CaO, and on the other hand, the temperature to which the particles are exposed during combustion is probably too low to promote the formation of reactive phases. This supposition is supported by the high LOI value of ~30 wt%.

The mechanical performance of the other two tested types of ash, namely, OSA-Ene(ef) and OSA-Auv(ef), is in about the same range as OSWA-Auv(ba). Their 56-day compressive and flexural strength is ~30–45 and ~6.0–7.0 MPa, respectively. However, in contrast to bottom ash, the former two both contain the β polymorph of dicalcium silicate, part of which is transformed to the γ polymorph solely in OSA-Auv(ef). In both types of electrostatic filter ash, milling increased reactivity measured with isothermal calorimetry from ~10 to ~100 J g^{-1} in OSA-Ene(ef) and from ~20 to ~150 J g^{-1} in OSA-Auv(ef); however, no significant impact on the mechanical properties of concrete was observed.

5. Conclusions

The principal aim of this study was to assess the feasibility of using OSA in concrete formulations for 3D printing and assess the effectiveness of collision milling as pretreatment. It was hypothesized that collision milling may activate the ash and that reduced particle size may be of benefit to printability.

Four types of OSA were collected, three extracted from the flue gasses (i.e., OSA-Ees(nid), OSA-Ene(ef), and OSA-Auv(ef)) and one from the bottom of the furnace (OSWA-Auv(ba)). The former were collision milled at 100 Hz, while the latter was milled at 30, 50, 100, and 130 Hz. The physical, chemical, and mineralogical characterization of ash was conducted. Furthermore, concrete formulations containing ash were derived from the reference formulation by replacing part of the cement with OSA and were tested for their mechanical performance. In terms of strength, two best-performing ash formulations, namely, OSA-Ees(nid) and its milled counterpart OSA-Ees(nid)/100, were also assessed for printability.

Overall, it can be concluded that the most suitable ash for use in concrete is OSA-Ees(nid); nevertheless, the results obtained on other types of ash also warrant further investigation. The second conclusion is that collision milling is probably a viable option only for bottom ash, which is too coarse for direct use as an SCM.

The first conclusion is supported by the following observations:

1. The particles of the ash extracted from the novel integrated desulfurizer, namely, OSA-Ees(nid), are mostly globular and smooth, resembling the cenospheres found in the FA from coal power plants. Such particles are formed at high combustion temperatures. The particles of the other two types of ash extracted from flue gasses and the bottom ash particles are predominantly angular;
2. The LOI value of OSA-Ees(nid) is <10 wt%, while in other types of ash, this value is significantly higher (~15–30 wt%). This indicates that in the case of the former, the combustion temperature is sufficiently high to burn the majority of kerogen and decompose the minerals;

3. The primary components of all tested ashes are SiO_2 and CaO. In ash extracted from flue gasses, they constitute ~20–30 and ~30–40 wt%, respectively, while in the bottom ash, they amount to ~5 and 50 wt% accordingly. In OSA-Ees(nid), the majority of these two oxides are consumed to form C_2S, which is found as an active β polymorph as well as a rather inert γ polymorph;
4. The compressive and flexural strength of the concrete formulation containing OSA-Ees(nid) was approximately the same as found in the reference formulation, amounting to ~60 and ~7 MPa at 56 days, respectively.

The second conclusion is supported by the following observations:

5. The size of the OSA-Ees(nid) particles is, on average, somewhat <10 μm and, overall, this ash is finer than CEM I, even before the pretreatment. Milling at 100 Hz only reduces the particles >10 μm, thus increasing the peak in the PSD curve at ~6 μm from ~6 to ~8 wt%;
6. In the case of the other three types of ash, which are coarser than CEM I, the milling shifts the PSD curve peak towards 10 μm, so that the overall results indicate that milling is effective only for particles >10 μm. The resulting change is significant only in the case of OSWA-Auv(ba);
7. Collision milling of the three types of flue gas ash resulted in a more than seven-fold increase of reactivity measured with the isothermal calorimetry. Namely, the released heat increased from ~10–20 J g^{-1} measured before milling to ~100–150 J g^{-1} after milling at 100 Hz;
8. Despite the increased reactivity measured by isothermal calorimetry, the mechanical properties of concrete formulations did not significantly improve when milled ash was used compared to their untreated counterparts. The only significant difference was found in OSWA-Auv(ba);
9. Concrete formulations incorporating either OSA-Ees(nid) or OSA-Ees(nid)/100 were checked for printability on a laboratory-scale gantry printer. No significant differences between the two were observed in the slug and the direct buildability tests. The yield stress calculated from the slug test was in a narrow range between ~1000 and 1200 Pa, including the reference formulation, while the yield stress calculated from the direct buildability test of the three formulations was between ~1500 and 2000 Pa.

Based on the findings of this study, future work will focus on using OSA-Ees(nid) in concrete formulations for 3D printing. Collision milling will not be further pursued in combination with this ash. First, the optimization of printable concrete formulations will be performed using screening methods such as measuring mechanical properties on cast specimens and optimizing the workability using the flow table, slug, and direct buildability tests. The optimized formulation will be assessed in detail for its mechanical properties, durability, and printability by adopting the methodologies developed by the technical committees (TCs) of the *International Union of Laboratories and Experts in Construction Materials, Systems, and Structures* (RILEM) [45], namely the TC 303-PFC *performance requirements and testing of fresh printable cement-based materials,* and the TC 304-ADC *assessment of additively manufactured concrete materials and structures*. One set of the results has already been submitted for publication [46]. Furthermore, the Life Cycle Assessment (LCA) and the Life Cycle Cost Assessment (LCCA) will be conducted for the optimized formulation.

In conclusion, the importance of this research for infrastructural projects should also be outlined since these projects consume a significant proportion of concrete and, in contrast to residential buildings, are expected to have a longer service life often under harsher conditions. Therefore, the challenge of using new types of cement and non-conventional SCMs in concrete for infrastructures will have to be addressed. This includes the nuclear power plants where concrete features heavily and is thus addressed by several research

projects dealing with nuclear materials, such as Orient-NM [47], Connect-NM [48], and Aces [49]. On the other hand, the main benefit of 3D printing structural elements is in the optimization of geometry, leading to large material savings. Two full-scale showcase infrastructural projects have already been executed. Namely, 4.5 m high water tanks with a diameter of 7 m were printed in Kuwait with 25 % material savings compared to tanks built with conventional technology [50]. The other showcase project is the prototype of the wind turbine tower printed in Denmark [51]. Furthermore, shortages in the labor market and the scale of demand for new infrastructures will necessitate automation and digital fabrication.

Author Contributions: Conceptualization, L.H., M.Š. (Mateja Štefančič), M.Š. (Māris Šinka), E.Š. and L.K.B.; methodology, L.H., M.Š. (Mateja Štefančič), M.Š. (Māris Šinka), E.Š. and B.M.; formal analysis, L.H., V.Z.S., M.Š. (Māris Šinka) and A.S.; investigation, M.Š. (Mateja Štefančič), K.Š., V.Z.S., A.S., G.Š., B.M. and L.K.B.; writing—original draft preparation, L.H. and A.S.; visualization, L.H. and A.S.; writing—review and editing, L.K.B.; data curation, K.Š.; project administration, M.Š. (Māris Šinka), E.Š. and L.K.B.; funding acquisition, L.H., M.Š. (Māris Šinka) and E.Š. All authors have read and agreed to the published version of the manuscript.

Funding: This research was funded through the transnational M-ERA.NET Joint Call 2022, project title "*Transforming waste into high-performance 3D printable cementitious composite*," acronym: Transition, funding period 2023–2026, https://www.m-era.net/home (accessed on 29 December 2024). Authors affiliated with the *Slovenian National Building and Civil Engineering Institute* acknowledge the co-funding of the Slovenian part of the transnational project by the *Ministry of Higher Education, Science and Innovation of the Republic of Slovenia*, under contract number C3360-25-452009.

Data Availability Statement: The data set is available in the OSF repository https://doi.org/10.17605/OSF.IO/MWF9N.

Acknowledgments: The authors acknowledge the guidance kindly provided by Diana Bajare and the keen support of Eva Dzene.

Conflicts of Interest: The authors declare no conflicts of interest. The funders had no role in the design of the study; in the collection, analyses, or interpretation of data; in the writing of the manuscript; or in the decision to publish the results.

References

1. Wang, N.; Xu, Z.; Liu, Z. Innovation in the construction sector: Bibliometric analysis and research agenda. *J. Eng. Technol. Manag.* **2023**, *68*, 101747. [CrossRef]
2. Reichstein, T.; Salter, A.J.; Gann, D.M. Last among equals: A comparison of innovation in construction, services and manufacturing in the UK. *Constr. Manag. Econ.* **2005**, *23*, 631–644. [CrossRef]
3. Sawhney, A.; Riley, M.; Irizarry, J. *Construction 4.0: An Innovation Platform for the Built Environment*, 1st ed.; Sawhney, A., Riley, M., Irizarry, J., Eds.; Routledge: Abingdon, OX, UK; New York, NY, USA, 2020.
4. Sivam, A.; Trasente, T.; Karuppannan, S.; Chileshe, N. The impact of an ageing workforce on the construction industry in Australia. In *Valuing People in Construction*, 1st ed.; Emuze, F., Smallwood, J., Eds.; Routledge: Abingdon, OX, UK; New York, NY, USA, 2017.
5. Clarke, L.; Michielsens, E.; Snijders, S.; Wall, C. *'No More Softly, Softly': Review of Women in the Construction Workforce*; University of Westminster: London, UK, 2015.
6. French, E.; Strachan, G. Women in the construction industry: Still the outsiders. In *Valuing People in Construction*, 1st ed.; Emuze, F., Smallwood, J., Eds.; Routledge: Abingdon, OX, UK; New York, NY, USA, 2017.
7. Wierzbicki, M.; de Silva, C.W.; Krug, D.H. BIM—History and trends. In Proceedings of the International Conference on Construction Applications of Virtual Reality, Weimar, Germany, 3–4 November 2011.
8. Borkowski, A.S. Evolution of BIM: Epistemology, genesis and division into periods. *J. Inf. Technol. Constr.* **2023**, *28*, 646–661. [CrossRef]
9. Ma, G.; Buswell, R.; Leal da Silva, W.R.; Wang, L.; Xu, J.; Jones, S.Z. Technology readiness: A global snapshot of 3D concrete printing and the frontiers for development. *Cem. Concr. Res.* **2022**, *156*, 106774. [CrossRef]
10. Wangler, T.; Lloret, E.; Reiter, L.; Hack, N.; Gramazio, F.; Kohler, M.; Bernhard, M.; Dillenburger, B.; Buchli, J.; Roussel, N.; et al. Digital concrete: Opportunities and challenges. *RILEM Tech. Lett.* **2016**, *1*, 67–75. [CrossRef]

11. Buswell, R.A.; Leal de Silva, W.R.; Jones, S.Z.; Dirrenberger, J. 3D printing using concrete extrusion: A roadmap for research. *Cem. Concr. Res.* **2018**, *112*, 37–49. [CrossRef]
12. Wangler, T.; Pileggi, R.; Gürel, S.; Flatt, R.J. A chemical process engineering look at digital concrete processes: Critical step design, inline mixing, and scaleup. *Cem. Concr. Res.* **2022**, *155*, 106782. [CrossRef]
13. Bos, F.P.; Menna, C.; Pradena, M.; Kreiger, E.; da Silva, W.R.L.; Rehman, A.U.; Weger, D.; Wolfs, R.J.M.; Zhang, Y.; Ferrara, L.; et al. The realities of additively manufactured concrete structures in practice. *Cem. Concr. Res.* **2022**, *156*, 106746. [CrossRef]
14. Kreiger, M.; Kreiger, E.; Mansour, S.; Monkman, S.; Delavar, M.A.; Sideris, P.; Roberts, C.; Friedell, M.; Platt, S.; Jones, S. Additive construction in practice—Realities of acceptance criteria. *Cem. Concr. Res.* **2024**, *186*, 107652. [CrossRef]
15. Scrivener, K.; Martirena, F.; Bishnoi, S.; Maity, S. Calcined clay limestone cements (LC3). *Cem. Concr. Res.* **2018**, *114*, 49–56. [CrossRef]
16. Scrivener, K.L.; John, V.M.; Gartner, E.M. Eco-efficient cements: Potential economically viable solutions for a low-CO_2 cement-based materials industry. *Cem. Concr. Res* **2018**, *114*, 2–26. [CrossRef]
17. Kahru, A.; Põllumaa, L. Environmental hazard of the waste streams of Estonian oil shale industry: An ecotoxicological review. *Oil Shale* **2006**, *23*, 53. [CrossRef]
18. Velts, O.; Uibu, M.; Kallas, J.; Kuusik, R. Waste oil shale ash as a novel source of calcium for precipitated calcium carbonate: Carbonation mechanism, modeling, and product characterization. *J. Hazard. Mater.* **2011**, *195*, 139–146. [CrossRef]
19. Usta, M.C.; Yörük, C.R.; Hain, T.; Paaver, P.; Snellings, R.; Rozov, E.; Gregor, A.; Kuusik, R.; Trikkel, A.; Uibu, M. Evaluation of new applications of oil shale ashes in building materials. *Minerals* **2020**, *10*, 765. [CrossRef]
20. Smadi, M.M.; Haddad, R.H. The use of oil shale ash in Portland cement concrete. *Cem. Concr. Compos.* **2003**, *25*, 43–50. [CrossRef]
21. Al-Hamaiedh, H.; Maaitah, O.; Mahadin, S. Using oil shale ash in concrete binder. *Electron. J. Geotech. Eng.* **2010**, *15*, 601–608.
22. Raado, L.-M.; Hain, T.; Liisma, E.; Kuusik, R. Composition and properties of oil shale ash concrete. *Oil Shale* **2014**, *31*, 147–160. [CrossRef]
23. *EVS 927:2018*; Burnt Shale for Building Materials. Specification, Performance and Conformity. Estonian Centre for Standardisation and Accreditation: Tallinn, Estonia, 2018.
24. Sobolev, K.; Gutiérrez, M.F. How nanotechnology can change the concrete world (part two): Successfully mimicking nature's bottom-up construction processes is one of the most promising directions. *Am. Ceram. Soc. Bull.* **2005**, *84*, 16–20.
25. Hanžič, L.; Šter, K.; Štefančič, M. Implementing the excess paste concept for a systematic mix design of printable concrete. In Proceedings of the Supplementary Conference Proceedings: Fourth RILEM International Conference on Concrete and Digital Fabrication—Digital Concrete 2024, Munchen, Germany, 4–6 September 2024.
26. Tümanok, A.; Kulu, P.; Tümanok, A. Treatment of different materials by disintegrator systems. *Proc. Est. Acad. Sci.* **1999**, *5*, 222–242.
27. Bumanis, G.; Bajare, D. Compressive strength of cement mortar affected by sand microfiller obtained with collision milling in disintegrator. *Procedia Eng.* **2017**, *172*, 149–156. [CrossRef]
28. *SIST EN 1097-5:2008*; Tests for Mechanical and Physical Properties of Aggregates—Part 5: Determination of the Water Content by Drying in a Ventilated Oven. Slovenian Institute for Standardization: Ljubljana, Slovenia, 2008.
29. *SIST EN 1097-7:2023*; Tests for Mechanical and Physical Properties of Aggregates—Part 7: Determination of the Particle Density of Filler—Pyknometer Method. Slovenian Institute for Standardization: Ljubljana, Slovenia, 2023.
30. *ISO 13320:2020*; Particle Size Analysis—Laser Diffraction Methods. International Organization for Standardization: Vernier (Geneva), Switzerland, 2020.
31. *EN 196-2:2013*; Methods of Testing Cement—Part 2: Chemical Analysis of Cement. European Committee for Standardization: Brussels, Belgium, 2013.
32. *SIST EN 451-1:2017*; Method for Testing Fly Ash—Part 1: Determination of Free Calcium Oxide Content. Slovenian Institute for Standardization: Ljubljana, Slovenia, 2017.
33. *EN 196-3:2016*; Methods of Testing Cement—Part 3: Determination of Setting Times and Soundness. European Committee for Standardization: Brussels, Belgium, 2016.
34. *EN 450-1:2012*; Fly Ash for Concrete Definition, Specifications and Conformity Criteria. European Committee for Standardization: Brussels, Belgium, 2012.
35. *ASTM C1897-20*; Standard Test Methods for Measuring the Reactivity of Supplementary Cementitious Materials by Isothermal Calorimetry and Bound Water Measurement. ASTM International: Philadelphia, PA USA, 2020.
36. Stefanidou, M.; Kesikidou, F.; Konopisi, S.; Vasiadis, T. Investigating the suitability of waste glass as a supplementary binder and aggregate for cement and concrete. *Sustainability* **2023**, *15*, 3796. [CrossRef]
37. *EN 1015-3:1999*; Methods of Test for Mortar for Masonry. Determination of Consistence of Fresh Mortar (by Flow Table). European Committee for Standardization: Brussels, Belgium, 1999.
38. *EN 1015-11:2019*; Methods of Test for Mortar for Masonry. Determination of Flexural and Compressive Strength of Hardened Mortar. European Committee for Standardization: Brussels, Belgium, 2019.

39. Ducoulombier, N.; Carneau, P.; Mesnil, R.; Demont, L.; Caron, J.-F.; Roussel, N. 'The Slug Test': Inline assessment of yield stress for extrusion-based additive manufacturing. In *Second RILEM International Conference on Concrete and Digital Fabrication*, 1st ed.; Bos, F.P., Lucas, S.S., Wolfs, R.J.M., Salet, T.A.M., Eds.; Springer: Cham, Switzerland, 2020; pp. 216–224. [CrossRef]
40. Suiker, A.S.J.; Wolfs, R.J.M.; Lucas, S.M.; Salet, T.A.M. Elastic buckling and plastic collapse during 3D concrete printing. *Cem. Concr. Res.* **2020**, *135*, 106016. [CrossRef]
41. Tao, Y.; Ren, Q.; Lesage, K.; Van Tittelboom, K.; Yuan, Y.; De Schutter, G. Shape stability of 3D printable concrete with river and manufactured sand characterized by squeeze flow. *Cem. Concr. Compos.* **2022**, *133*, 104674. [CrossRef]
42. *EN 12350-6:2019*; Testing Fresh Concrete—Part 6: Density. European Committee for Standardization: Brussels, Belgium, 2019.
43. Labus, M.; Matyasik, I.; Ziemianin, K. Thermal decomposition processes in relation to the type of organic matter, mineral and maceral composition of menilite shales. *Energies* **2023**, *16*, 4500. [CrossRef]
44. Wang, Q.; Li, F.; Shen, X.; Shi, W.; Li, X.; Guo, Y.; Xiong, S.; Zhu, Q. Relation between reactivity and electronic structure for α'L-, β- and γ-dicalcium silicate: A first-principles study. *Cem. Concr. Res.* **2014**, *57*, 28–32. [CrossRef]
45. RILEM. International Union of Laboratories and Experts in Construction Materials, Systems and Structures. Available online: https://www.rilem.net/ (accessed on 15 November 2024).
46. Sapata, A.; Sinka, M.; Šahmenko, G.; Korat Bensa, L.; Hanžič, L.; Šter, K.; Rucevskis, S.; Bajare, D.; Bos, F.P. Establishing benchmark properties for 3d-printed concrete: A study of printability, strength, and durability. *J. Compos. Sci.* 2024, *submitted*.
47. Orient-NM. Organisation of the European Research Community on Nuclear Materials, Euratom Research and Training Programme. Available online: https://www.eera-jpnm.com/orient-nm/ (accessed on 29 December 2024).
48. Connect-NM. Coordination of the European Nuclear Materials Community for Energy Innovation, Euratom Research and Training Programme. Available online: https://indico.scc.kit.edu/event/3644/attachments/7119/11266/5_Innumat_WS_23_Connect-nminnumatb_Malerba.pdf (accessed on 17 December 2024).
49. Aces. Towards Improved Assessment of Safety Performance for LTO of Nuclear Civil Engineering Structures, Euratom Research and Training Programme. Available online: https://aces-h2020.eu/ (accessed on 15 November 2024).
50. Cobod. World's First 3D Printed Large Concrete Tanks Made with Materials Savings of 25%, Press release 05/03/2024. Available online: https://cobod.com/worlds-first-3d-printed-large-concrete-tanks-made-with-materials-savings-of-25/ (accessed on 23 December 2024).
51. Cobod. The Revolutionary Impact of 3D Printing on Industries, Blog 27/04/2023. Available online: https://cobod.com/the-revolutionary-impact-of-3d-printing-on-industries/ (accessed on 23 December 2024).